Amyloid precursor protein (APP) traffics from the cell surface via endosomes for amyloid β (Aβ) production in the *trans*-Golgi network

Regina Wai-Yan Choy[a,b], Zhiliang Cheng[a,b], and Randy Schekman[a,b,1]

[a]Department of Molecular and Cell Biology and [b]Howard Hughes Medical Institute, University of California, Berkeley, CA 94720

Contributed by Randy Schekman, May 23, 2012 (sent for review January 14, 2012)

Amyloid precursor protein (APP) is processed sequentially by the β-site APP cleaving enzyme and γ-secretase to generate amyloid β (Aβ) peptides, one of the hallmarks of Alzheimer's disease. The intracellular location of Aβ production—endosomes or the *trans*-Golgi network (TGN)—remains uncertain. We investigated the role of different postendocytic trafficking events in $Aβ_{40}$ production using an RNAi approach. Depletion of Hrs and Tsg101, acting early in the multivesicular body pathway, retained APP in early endosomes and reduced $Aβ_{40}$ production. Conversely, depletion of CHMP6 and VPS4, acting late in the pathway, rerouted endosomal APP to the TGN for enhanced APP processing. We found that VPS35 (retromer)-mediated APP recycling to the TGN was required for efficient $Aβ_{40}$ production. An interruption of the bidirectional trafficking of APP between the TGN and endosomes, particularly retromer-mediated retrieval of APP from early endosomes to the TGN, resulted in the accumulation of endocytosed APP in early endosomes with reduced APP processing. These data suggest that $Aβ_{40}$ is generated predominantly in the TGN, relying on an endocytosed pool of APP recycled from early endosomes to the TGN.

endocytosis | endosomal sorting complexes required for transport pathway | vesicular traffic | protein sorting | proteolytic processing

Alzheimer's disease is a common neurodegenerative disorder that is characterized by the presence of amyloid β (Aβ) peptide-containing plaques in the brain. In the amyloidogenic pathway, amyloid precursor protein (APP) undergoes sequential steps of proteolytic processing, first by the β-site APP cleaving enzyme (BACE), and then by γ-secretase to generate Aβ peptides. All these players in the amyloidogenic pathway are transmembrane proteins that traffic through the secretory pathway as well as the endocytic pathway. The subcellular compartment in which APP is processed to generate Aβ has remained controversial. It is possible that APP could be cleaved into Aβ in any of the organelles along these pathways, including the endoplasmic reticulum (ER); the Golgi apparatus; the plasma membrane; early, late, or recycling endosomes; and the lysosome (1, 2). Although γ-secretase localizes predominantly in the ER (3, 4), we previously showed by using a cell-free COPII vesicle budding assay that its catalytic subunit presenilin-1 exited the ER without undergoing the endoproteolysis required to maximize γ-secretase activity, suggesting that Aβ production is likely to occur in a post-ER compartment (5). Along the secretory pathway, several groups suggested the Golgi apparatus or the *trans*-Golgi network (TGN) as the major Aβ-producing organelle (6–8); whereas the plasma membrane has been demonstrated as the predominant site for nonamyloidogenic processing of APP by α-secretase (9).

The endocytic pathway has also been shown to play significant roles in the proper processing of APP into Aβ. Inhibition of endocytosis by expression of a dominant-negative mutant of dynamin or by mutation of the endocytic sorting signal of APP reduces Aβ production (10, 11). In addition, it is generally believed that the first enzymatic cleavage of APP by BACE to form the membrane-bound APP C-terminal fragment (β-CTF), an intermediate substrate for γ-secretase to produce Aβ, occurs predominantly in early endosomes (12, 13). Hence, converging evidence confirmed the importance of the endocytic pathway in the regulation of Aβ production. To date, there has been limited detailed analysis dissecting the different downstream steps following endocytosis to reveal the actual location in which Aβ is produced. Potential sites include early or late endosomes or the multivesicular body (MVB) involved in sorting transmembrane proteins for degradation in the lysosome, as well as along the retrograde pathway that mediates the recycling of endosomal proteins to the TGN.

We investigated the importance of different postendocytic trafficking steps in the production of $Aβ_{40}$ by using an RNAi approach and observed distinct effects in the early and late stages of the MVB pathway on $Aβ_{40}$ production as well as on APP localization. Furthermore, we demonstrated that the majority of APP is processed in the TGN to produce $Aβ_{40}$, with a requirement for the retromer to sustain protein recycling from endosomes to the TGN.

Results

Depletion of Endosomal Sorting Complexes Required for Transport Pathway Alters $Aβ_{40}$ Production and Redistributes APP. Membrane proteins at the plasma membrane are sorted into the MVB and lysosomal degradation pathways by the endosomal sorting complexes required for transport (ESCRT) pathway (14, 15). The ESCRT-0 complex mediates sorting and concentration of cargoes to this pathway, the ESCRT-I and ESCRT-II complexes are important for endosomal membrane budding, the ESCRT-III complex is involved in membrane scission to form internal vesicles within MVBs, and the AAA+ ATPase VPS4 disassembles and recycles ESCRT-III components to sustain subsequent rounds of the pathway (14, 15). To ascertain the involvement of the endosomal MVB pathway happening downstream of the endocytic event in APP processing, we investigated the effects of depleting different ESCRT complex subunits on $Aβ_{40}$ production and APP localization.

We performed shRNA-based knockdown of Hrs (ESCRT-0), Tsg101 (ESCRT-I), CHMP6 (ESCRT-III), and VPS4A/B in HEK293 cells stably expressing APP_{695} (Fig. 1 *A* and *B*), and analyzed the changes in secreted $Aβ_{40}$ levels in the culture media by ELISA. We did not measure secreted $Aβ_{42}$ because of the low abundance of this cleaved form in our cell line. Depletion of the indicated individual components of each ESCRT complex resulted in degradation of the respective ESCRT complex (16–20). Depletion of Hrs or Tsg101 led to 23 ± 3% and 40 ± 5% decreases in $Aβ_{40}$, respectively, whereas an increase in $Aβ_{40}$ to

Author contributions: R.W.-Y.C. and R.S. designed research; R.W.-Y.C. and Z.C. performed research; R.W.-Y.C. and R.S. analyzed data; and R.W.-Y.C., Z.C., and R.S. wrote the paper.

The authors declare no conflict of interest.

[1]To whom correspondence should be addressed. E-mail: schekman@berkeley.edu.

See Author Summary on page 11914 (volume 109, number 30).

This article contains supporting information online at www.pnas.org/lookup/suppl/doi:10.1073/pnas.1208635109/-/DCSupplemental.

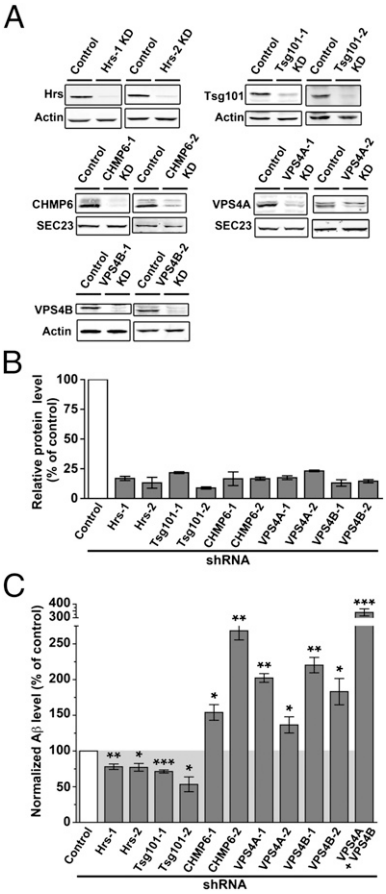

Fig. 1. ESCRT depletion affects $A\beta_{40}$ production. (*A*) HEK293 cells stably expressing APP_{695} were transfected with empty vector pSUPER (control) or two shRNA constructs directed toward distinct regions of mRNA sequences of Hrs, Tsg101, CHMP6, VPS4A, or VPS4B (KD). Cells were lysed at 120 h posttransfection, and proteins were analyzed by immunoblot. Actin or SEC23A were used as loading controls. (*B*) Relative protein levels in shRNA knockdown cells, as a percentage of the control (set as 100%), were quantified by the LI-COR Odyssey Infrared Imaging System (mean ± SEM; $n \geq 3$). (*C*) Culture media conditioned from 96 h to 120 h posttransfection were subjected to $A\beta_{40}$ ELISA analysis. Relative normalized $A\beta_{40}$ levels as a percentage of the control (set as 100%) were plotted as mean ± SEM ($n \geq 3$; $^*P < 0.05$, $^{**}P < 0.01$, and $^{***}P < 0.001$).

varying degrees was observed upon depletion of CHMP6 or VPS4A/B, with more than a threefold increase in the $A\beta_{40}$ level in double knockdown of VPS4A and VPS4B (Fig. 1*C*). The ESCRT complexes act at different stages in the formation of an MVB (14, 15); thus, depleting subunits may differentially affect the intracellular trafficking and steady-state distribution of APP and the processing proteases, leading to differences in the efficiency of $A\beta_{40}$ production.

To correlate the changes in the $A\beta_{40}$ levels with the steady-state distribution of APP upon depletion of ESCRT subunits, we used immunofluorescence microscopy to visualize APP colocalization with different organelle markers. We used an antibody that recognizes the C terminal of human APP_{695} to immunostain for intracellular APP. This antibody is able to detect the full-length form (Fig. S1) as well as the β-CTF fragment of APP (Fig. S2). We did not have a robust staining of β-CTF using a β-CTF–specific neoepitope antibody (21) as a result of the low abundance of the rapidly processed and/or degraded β-CTF fragments (Fig. S2). However, we expect β-CTF would traffic in a similar manner as full-length APP because both species have the same intact cytosolic domain that contains sorting signals for ESCRTs as well as other sorting factors such as retromer and adaptor protein complex-4 (AP-4) (8). Therefore, we reason that changes in the localization of full-length APP upon different knockdowns could also reflect the changes in trafficking of the β-CTF fragments.

In control cells, APP predominantly localized to the TGN as visualized by the TGN marker Golgin 97 (55 ± 7%; Fig. 2 *A–D*), with only a subset of APP (9 ± 2%) colocalized with the early endosome marker EEA1 (Fig. 2 *E–H*) and the remaining signals of APP distributed throughout the cytosol, the ER, and the plasma membrane. Interestingly, in Hrs- or Tsg101-depleted cells, APP was redistributed from the TGN to enlarged ring-like structures of varying sizes that were labeled by EEA1 (Hrs, 21 ± 5%; Tsg101, 26 ± 6%; Fig. 2 *I–P*). With the deficiency of these early ESCRT subunits, APP appeared to be retained in enlarged endosomal compartments that were defective in progression further along the MVB pathway, thus delaying APP transport to late endosomes, MVBs, and lysosomes, as well as its retrograde transport to the TGN. The decrease in the $A\beta_{40}$ levels accompanied by the accumulation of APP in these compartments suggested that $A\beta_{40}$ production may be less efficient in early endosomes, and that APP traffic beyond early endosomes was required to gain access to an organelle favorable for the generation of $A\beta_{40}$.

In CHMP6-, or VPS4A/B-depleted cells, APP localized predominantly to the TGN (CHMP6, 56 ± 6%; VPS4A, 54 ± 6%; VPS4B, 51 ± 6%; Fig. 2 *Q–AB*), which was comparable to the

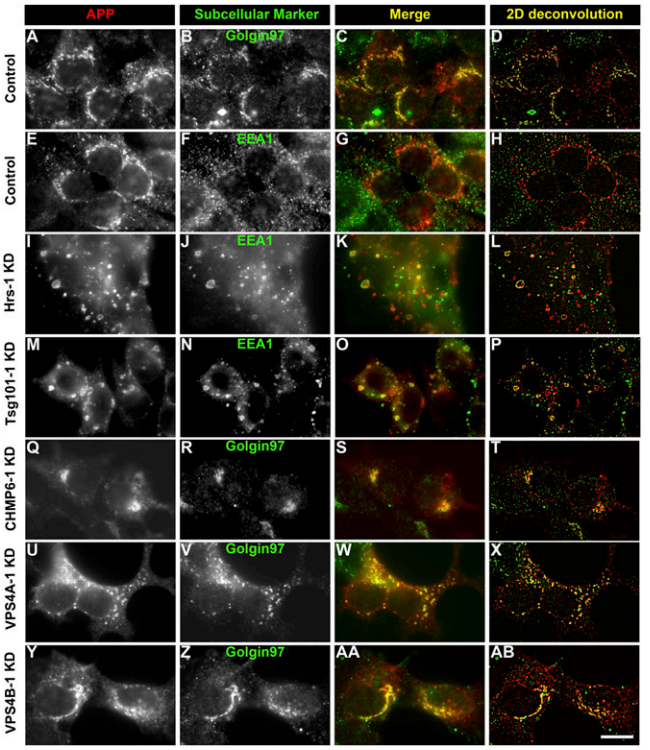

Fig. 2. ESCRT depletion affects steady-state APP localization. HEK293 cells stably expressing APP_{695} were transfected with empty vector pSUPER+GFP (control) or shRNA directed to Hrs, Tsg101, CHMP6, VPS4A, or VPS4B (KD). Cells were fixed at 120 h posttransfection and stained for APP and subcellular markers Golgin 97 or EEA1. Because pSUPER+GFP vector coexpressed both the shRNA and GFP, GFP signals were used to indicate which cells sustained knockdown. Representative cells with GFP signals are shown. Merged images were generated from the Alexa 568 channel (APP signals indicated by red) and the Alexa 647 channel (Golgin 97 or EEA signals indicated by green), or 2D deconvolved images from each channel; colocalization is indicated by yellow. (Scale bars: 10 μm.)

control cells (55 ± 7%; Fig. 2 *A–D*). We also observed some dispersal of the Golgi structures in VPS4A/B-depleted cells, which could be a general effect of VPS4A/B knockdown (Fig. 2 *V* and *Z*). We speculate that the enhancement in $A\beta_{40}$ levels upon late ESCRT depletion (Fig. 1*C*) might be attributed to a redirection of endocytosed APP to the TGN, which we believe to represent a favorable subcellular site for $A\beta_{40}$ production (6–8).

Endocytosed APP Is Redirected to TGN upon VPS4 Depletion. Increased $A\beta_{40}$ production in VPS4 or other late ESCRT-depleted cells with APP predominantly localized to the TGN could be a result of defective TGN export of APP caused by perturbation of the Golgi integrity (Fig. 2 *V* and *Z*), or the enhanced routing of APP from the endocytic pathway into the retrograde pathway directed toward the TGN. To distinguish between these possibilities, we performed a double knockdown of Hrs and VPS4A (Fig. 3 *A* and *B*), and assessed changes in APP localization and the $A\beta_{40}$ level. The steady-state localization of APP was redistributed to enlarged ring-like structures of varying sizes that were labeled by EEA1 (26 ± 10%; Fig. 3 *D*, *a–d*), similar to the observation in single Hrs-depleted cells (Fig. 2 *I–L*), accompanied by a decrease in TGN localization (12 ± 3%; Fig. 3 *D*, *e–h*). A 13 ± 2% decrease in $A\beta_{40}$ levels (Fig. 3*C*) was consistent with the notion that $A\beta_{40}$ was produced less efficiently in cells that display these enlarged early endosomal compartments. These results demonstrated that depletion of Hrs and VPS4A produced a phenotype similar to the depletion of Hrs alone, which suggested that the action of VPS4 in APP processing is exerted downstream of Hrs. Therefore, APP accumulation in the TGN in single VPS4A-depleted cells appears to have derived from an endosomal pool that was retrieved back to the TGN.

Retromer Depletion Reduces $A\beta_{40}$ Production. Two routes of retrograde traffic from endosomes to the TGN have been characterized: one from early and recycling endosomes and dependent on retromer but Rab9-independent, and another from late endosomes and dependent on Rab9 (22–24). Recent evidence suggests that endosome-to-TGN recycling of APP is retromer-dependent (25, 26). To confirm that retrieval of APP from endosomes to the TGN was important in the production of $A\beta_{40}$, we examined the early and late recycling routes by knockdown of VPS35 and Rab9A, respectively (Fig. 4 *A* and *B*). Depletion of a retromer core subunit VPS35 redistributed APP from the TGN to puncta that partially colocalized with EEA1 (28 ± 9%; Fig. 4*D*, *e–g*), but to a lesser extent with Golgin 97 (20 ± 3%; Fig. 4*D*, *a–d*) compared with the control (55 ± 7%; Fig. 2 *A–D*), suggesting that recycling of APP from the early endosomes to the TGN was defective. A 26 ± 3% decrease in the $A\beta_{40}$ level was measured in VPS35-depleted cells (Fig. 4*C*), which correlated well with the reduced localization of APP to the TGN. In contrast, in Rab9A-depleted cells, APP largely colocalized with Golgin 97 (57 ± 3%; Fig. 4*D*, *i–l*), with a subset of APP colocalized with EEA1 (12 ± 2%; Fig. 4*D*, *m–p*). This pattern was comparable to the APP distribution in control cells (Fig. 2 *A–H*), suggesting the retrograde transport of APP to the TGN was not impaired in Rab9A knockdown cells. Consistent with this, no significant change in the $A\beta_{40}$ level was observed (Fig. 4*C*). However, we cannot definitely exclude an effect of Rab9 on APP processing because the knockdown was not complete and because of the existence of a Rab9B isoform. We conclude that retromer-dependent retrieval of APP from early endosomes to the TGN facilitates enhanced production of $A\beta_{40}$ peptides derived from the endocytic pool of APP.

Retrograde Transport of Endocytosed APP to TGN Is Required for $A\beta_{40}$ Production. Although our results were consistent with an endocytic origin of $A\beta_{40}$, a plausible alternative was that retromer-

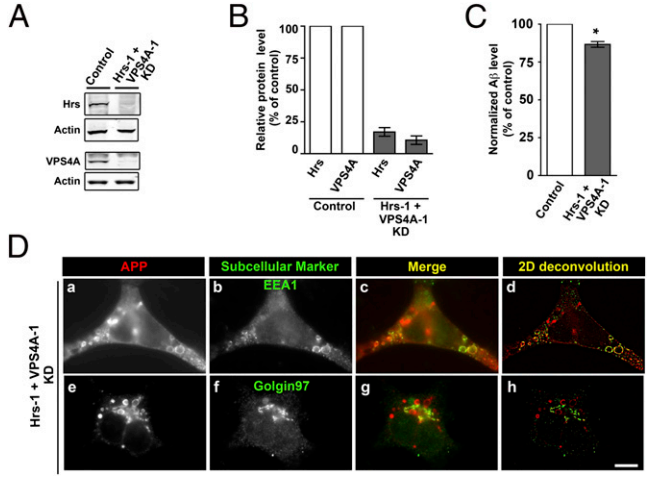

Fig. 3. Double knockdown of Hrs and VPS4A resembled single Hrs knockdown phenotypes. For *A–C*, experiments were performed as in Fig. 1, cells were transfected with empty vector (control) or pooled shRNA constructs (Hrs-1 and VPS4A-1) directed to Hrs and VPS4A (KD). (*A*) Immunoblot and (*B*) quantification of relative protein levels (mean ± SEM; $n = 3$), and (*C*) $A\beta_{40}$ ELISA analysis (mean ± SEM; $n = 3$; $^*P < 0.05$). (*D*) Experiments were performed as in Fig. 2, and cells were transfected with pooled pSUPER+GFP shRNA constructs (Hrs-1 and VPS4A-1) directed to Hrs and VPS4A (KD). Representative cells with GFP signals are shown. (Scale bars: 10 μm.)

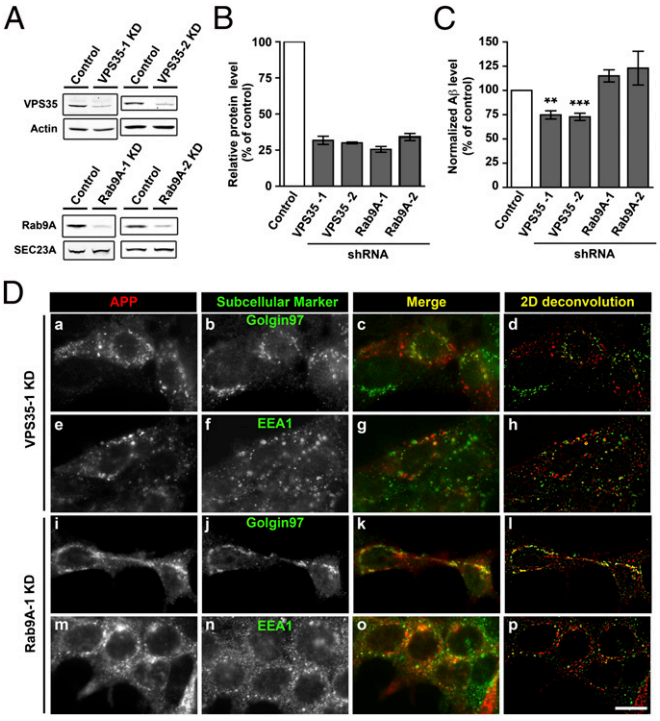

Fig. 4. VPS35 depletion delayed retrieval of APP to the TGN and Aβ production. For *A–C*, experiments were performed as in Fig. 1, and cells were transfected with empty vector (control) or two shRNA constructs directed to VPS35 or Rab9A (KD). (*A*) Immunoblot and (*B*) quantification of relative protein levels (mean ± SEM; $n = 3$), and (*C*) $A\beta_{40}$ ELISA analysis (mean ± SEM; $n \geq 3$; $^{**}P < 0.01$ and $^{***}P < 0.001$, only P values < 0.05 shown). (*D*) Experiments were performed as in Fig. 2, and cells were transfected with pSUPER+GFP shRNA directed to VPS35 or Rab9A (KD). Representative cells with GFP signals are shown. (Scale bars: 10 μm.)

dependent recycling from an early endosome was necessary to sustain $A\beta_{40}$ production from newly synthesized APP in transit through the TGN. Indeed, Burgos et al. proposed a direct TGN-to-endosome route for APP mediated by the direct interaction of APP with AP-4 (8). Disruption of the interaction between the μ-subunit of AP-4 complex (AP-4 μ) and APP or depletion of AP-4 μ shifted the steady-state distribution of APP to the TGN with an increase in the Aβ level, consistent with a role for the TGN in APP processing (8). We repeated the AP-4 μ knockdown experiment in HEK293 cells expressing APP_{695} (Fig. 5 *A* and *B*), and we observed increased production of $A\beta_{40}$ (Fig. 5 *C*) and steady-state localization of APP to the TGN (55 ± 4%) (Fig. 5*D*, *a*–*d*). These results are consistent with those of Burgos et al. but do not necessarily demonstrate that APP cleaved in the TGN is derived from biosynthetic precursors en route to the cell surface (8).

To examine whether the recycled APP came from the cell surface-derived endocytic pool or from the biosynthetic pool, we performed a double knockdown of AP-4 μ and the retromer subunit VPS35 to block forward and retrograde trafficking between the TGN and the endosomes. If the majority of APP molecules cleaved in the TGN were of direct biosynthetic origin, we would expect the double knockdown and single AP-4 μ depletion to result in an increase in $A\beta_{40}$ production. In contrast, we observed a 32 ± 1% reduction in $A\beta_{40}$ production upon double depletion of AP-4 μ and VPS35. As expected, APP redistributed to enlarged ring-like EEA1-positive structures with varying sizes in the double knockdown (35 ± 14%; Fig. 5*D*, *i*–*l*), similar to the localization of APP in Hrs- or Tsg101-depleted cells, and with a corresponding decrease in APP localization in the TGN (10 ± 1%; Fig. 5*D*, *e*–*h*). This distribution was not observed in single knockdowns of AP-4 μ or VPS35. We suggest that disruption of bidirectional traffic of APP between the TGN and endosomes leads to efficient export of APP to the cell surface and subsequent accumulation of the precursor in an early endosome.

Our results support the conclusion of Burgos et al. that APP processing occurs in the TGN (8), but we suggest that the majority of APP substrate is retrieved from the cell surface.

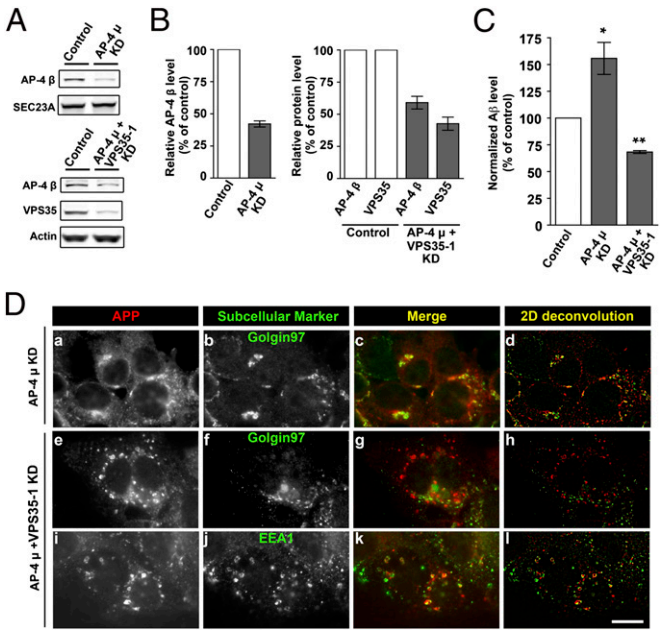

Fig. 5. Double knockdown of AP-4 μ and VPS35 retained APP in the early endosomes and reduced $A\beta_{40}$ production. For *A*–*C*, experiments were performed as in Fig. 1, and cells were transfected with empty vector (control) or shRNA directed to AP-4 μ or pooled shRNA constructs (AP-4 μ and VPS35-1) directed to AP-4 μ and VPS35-1 (KD) for double knockdown. (*A*) Immunoblot. Antibody against the β-subunit of AP-4 was used because β- and μ-subunits of AP-4 reside in the same hemicomplex; depletion of AP-4 μ should mirror the loss of AP-4 β. (*B*) Quantification of relative protein levels (mean ± SEM; $n = 3$) (*C*) $A\beta_{40}$ ELISA analysis (mean ± SEM; $n = 3$; $^*P < 0.05$ and $^{**}P < 0.01$). (*D*) Experiments were performed as in Fig. 2, and cells were transfected with pSUPER+GFP shRNA directed to AP-4 μ or pooled shRNA constructs (AP-4 μ and VPS35-1) directed to AP-4 μ and VPS35-1 (KD). Representative cells with GFP signals are shown. (Scale bars: 10 μm.)

Discussion

The location of APP processing to produce Aβ peptide has been ascribed to many organelles, including the ER, TGN, early and late endosomes, recycling endosomes, and the lysosome (1, 2). Recent evidence has focused on the TGN or endosomes (more specifically, early endosomes) as the locus of Aβ production. Both the TGN and early endosomes serve as sorting stations for proteins that traffic through the secretory and endocytic pathways, and they communicate with one another through a bidirectional flow of transport vesicles (22–24, 27, 28). The exact location of APP processing will depend on the balance of traffic of the precursor and the secretase enzymes. Thus, at least some of the disparate results may derive from variations in cell type and conditions of cell growth.

In our experimental system, by using HEK293 cells expressing APP_{695}, we demonstrated that the processing of APP into $A\beta_{40}$ occurs predominantly in the TGN. We observed a correlation between the increase in $A\beta_{40}$ and the accumulation of APP in the TGN, as shown by depleting the late ESCRT components CHMP6 or VPS4A/B, which rerouted APP from the endocytic pathway to the TGN (Fig. 1), or by depleting AP-4 μ to impede direct TGN-to-endosome trafficking of APP (Fig. 5). In contrast, reduced $A\beta_{40}$ levels were observed when there was a shift in steady-state localization of APP from the TGN to early endosomes, as shown by knockdown of the early ESCRT components Hrs or Tsg101 (Fig. 1) or by double knockdown of VPS35 and AP-4 μ (Fig. 5). Furthermore, we noted distinct effects on APP processing and trafficking upon depletion of subunits of different ESCRT complexes (Fig. 1). Depletion of early ESCRT subunits, such as Hrs and Tsg101, delayed APP exit from early endosomes. However, depletion of later ESCRT components, such as CHMP6 and VPS4A/B, promoted APP recycling from an endosome to the TGN. These results suggest that a block in an early ESCRT event impedes APP recycling from the early endosome, whereas a late event, such as in the VPS4-mediated recycling of ESCRT subunits, can be blocked without disabling recycling of APP.

Our findings based on the double knockdown of Hrs and VPS4 suggest that recycling from an endosome plays an important role in $A\beta_{40}$ production (Fig. 3). Endosomal proteins that recycled to the TGN could take two major routes, either via the retromer-dependent pathway from early endosomes or the Rab9-dependent pathway from late endosomes (22, 23). Recent evidence (25, 26) and our data on VPS35 depletion (Fig. 4) support a role for the retromer in the traffic of APP from early endosomes to the TGN. By using similar yet independent stable cell lines of HEK293 overexpressing APP_{695}, both Sullivan et al. (26) and our group showed consistent results of a decrease in $A\beta_{40}$ production upon VPS35 knockdown. On the contrary, Small et al. (29) has reported an increase in endogenous $A\beta_{40}$ level in HeLa cells after depletion of VPS35. The discrepancy could be a result of different origins of the cell types as well as the expression levels of APP. Rab9A depletion to block the alternative recycling path had no effect on APP processing (Fig. 4).

Our results suggest an endocytic origin of APP processed in the TGN. However, Burgos et al. suggested that biosynthetic APP directed to the endosome by the AP-4 complex might be the preferred substrate for Aβ production (8). We found that double knockdown of AP-4 μ and VPS35 resulted in reduced $A\beta_{40}$

production with APP redistributed to enlarged early endosomes (Fig. 5). This result argues that the majority of APP substrate for γ-secretase arrives via the cell surface, although it is likely that some biosynthetic APP cycling directly between endosomes and the TGN is processed without sampling the cell surface. Although we showed how the APP trafficking and localization were affected upon depletion of ESCRTs, retromer, and AP-4, it is possible that, at the same time these knockdowns could also affect the trafficking of BACE and γ-secretase, resulting in the changes in $A\beta_{40}$ level we observed.

Why does APP traffic to the plasma membrane before being retrieved via the retromer complex for proteolytic processing in the TGN? One possibility is that the BACE, which must process APP to β-CTF before γ-secretase acts to generate Aβ peptide, is localized primarily to early endosomes (12, 13). When APP has been processed by BACE in early endosomes, APP β-CTF could then be transported to the TGN for Aβ production.

Interestingly, the sortilin-related receptor SorLA was identified as a genetic risk factor for late-onset Alzheimer's disease (30). SorLA was shown to localize to the TGN and endosomes and to mediate APP traffic between these organelles (31, 32). However, the role of SorLA in anterograde or retrograde traffic between the TGN and endosomes has not been resolved (31–33). Importantly, depletion of SorLA increases Aβ production (30). Our results and those of Burgos et al. are most consistent with a role for SorLA in the traffic of APP from the TGN, rather than from an endosome (8).

In summary, we demonstrated that the retromer-dependent recycling pathway is important in the process of $A\beta_{40}$ production, possibly by maintaining the balance of APP traffic between the TGN and endosomes (Fig. 6). We suggest that a necessary pass of internalized APP through the BACE compartment en route to γ-secretase in the TGN organizes the secretory and endocytic pathways in this processing event.

Materials and Methods

Antibodies. Mouse monoclonal antibodies used were anti-Hrs (A-5; Enzo Life Sciences), anti-Tsg101 (4A10; Genetex), anti-Rab9 (mab9; EMD Chemicals), anti-Golgin 97 (CDF4; Life Technologies), anti-EEA1 (no. 14; BD Transduction Laboratories), anti-Actin (C4; MP Biomedicals), anti-APP β-CTF neoepitope (3D6; gift from S. S. Sisodia, University of Chicago, Chicago, IL), and anti-APP N-terminal (P2-1; gift from S. S. Sisodia, University of Chicago). Rabbit polyclonal antibodies used were anti-CHMP6 (gift from W. I. Sundquist, University of Utah, Salt Lake City, UT), anti-VPS4A (gift from W. I. Sundquist, University of Utah), anti-VPS4B (gift from W. I. Sundquist, University of Utah), anti-β subunit of AP-4 (gift from M. S. Robinson; University of Cambridge, Cambridge, United Kingdom), anti-SEC23A (gift from J. P. Paccaud, Drugs of Neglected Diseases Initiative, Geneva, Switzerland), and anti-APP C-terminal (Sigma-Aldrich). Goat polyclonal anti-VPS35 antibody was obtained from Imgenex. IRDye 680 and 800 secondary antibodies (LI-COR) were used for immunoblotting analysis. Alexa Fluor 568- and 647-conjugated secondary antibodies (Life Technologies) were used for immunofluorescence microscopy.

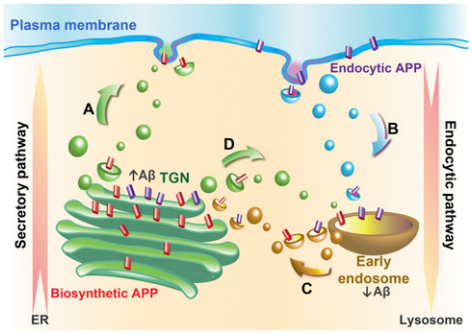

Fig. 6. Model for APP trafficking in $A\beta_{40}$ production. (*A*) For APP to be cleaved efficiently into $A\beta_{40}$ in the TGN, newly synthesized APP (red) at the ER first traffics along the secretory pathway via the TGN to the plasma membrane. (*B*) APP is then internalized via endocytosis to reach early endosomes. (*C*) Next, the endocytic pool of APP (purple) is recycled to the TGN in a retromer-dependent manner, where Aβ is produced. (*D*) The biosynthetic pool of APP (red) in the TGN can also traffic directly to endosomes in a process mediated by the AP-4 complex (*C*) and be retrieved back to the TGN in a retromer-dependent manner for Aβ production.

Cell Line. Full-length cDNA of human APP_{695} was cloned into pCI-neo mammalian expression vector (Promega) and transfected in HEK293 cells (American Type Culture Collection). Cells were selected on Geneticin/G418 (Life Technologies) and subcloned. Stable HEK293 cells expressing APP_{695} were cultured in DMEM/high glucose/GlutaMAX (Life Technologies) with the addition of 10% FBS (HyClone), 0.1 mM NEAA (Life Technologies), and 650 μg/mL Geneticin/G418 (Life Technologies), and maintained in a humidified incubator with 5% CO_2 at 37 °C.

RNAi Constructs. The mRNA sequences of human Hrs, Tsg101, CHMP6, VPS4A, VPS4B, VPS35, and Rab9A were used to design shRNA for specific gene silencing by using the siDirect 2.0 Web server and siRNA Target Finder software from Ambion.

Custom-made 62-nt DNA oligonucleotides were designed to contain a 19-nt sense strand target sequence that was linked to the 19-nt reverse complement antisense sequence by a short spacer region (5′-TTCAAGAGA-3′), followed by the RNA polymerase III termination sequence (5′-TTTTTT-3′), with the addition of BglII and BamHI restriction enzyme sites flanking the 5′ and 3′ ends, respectively.

Two pairs of complementary oligonucleotides directed toward distinct regions of mRNA sequences of each knockdown target was synthesized (Integrated DNA Technologies) as follows: 5′-GATCGAGACAAGTGGAGGTAAACTTCAAGAGAGTTTACCTCCACTTGTCTCTTTTTTGGAAA-3′ and 5′-AGCTTTTCCAAAAAAGAGACAAGTGGAGGTAAACTCTCTTGAAGTTTACCTCCACTTGTCTC-3′ for Hrs-1; 5′-GATCCCTGTACTCTTCACCTGTGTTCAAGAGACACAGGTGAAGAGTACAGGTTTTTTGGAAA-3′ and 5′- AGCTTTTCCAAAAAACCTGTACTCTTCACCTGTGTCTCTTGAACACAGGTGAAGAGTACAGG-3′ for Hrs-2; 5′-GATCCCTCCAGTCTTCTCTCGTCTTCAAGAGAGACGAGAGAAGACTGGAGGTTTTTTGGAAA-3′ and 5′- AGCTTTTCCAAAAAACCTCCAGTCTTCTCTCGTCTCTCTTGAAGACGAGAGAAGACTGGAGG-3′ for Tsg101-1; 5′- GATCGAAGTAGCCGAGGTTGATATTCAAGAGATATCAACCTCGGCTACTTCTTTTTTGGAAA-3′ and 5′- AGCTTTTCCAAAAAAGAAGTAGCCGAGGTTGATATCTCTTGAATATCAACCTCGGCTACTTC-3′ for Tsg101-2; 5′-GATCATGAGTGTCTGAACAAGATTTCAAGAGAATCTTGTTCAGACACTCATTTTTTTGGAAA-3′ and 5′- AGCTTTTCCAAAAAAATGAGTGTCTGAACAAGATTCTCTTGAAATCTTGTTCAGACACTCAT-3′ for CHMP6-1; 5′-GATCGCGCAATCACTCAGGAACATTCAAGAGATGTTCCTGAGTGATTGCGCTTTTTTGGAAA-3′ and 5′- AGCTTTTCCAAAAAAGCGCAATCACTCAGGAACATCTCTTGAATGTTCCTGAGTGATTGCGC-3′ for CHMP6-2; 5′- GATCGGATTATTTACGAAGCAAATTCAAGAGATTTGCTTCGTAAATAATCCTTTTTTGGAAA-3′ and 5′- AGCTTTTCCAAAAAAGGATTATTTACGAAGCAAATCTCTTGAATTTGCTTCGTAAATAATCC-3′ for VPS4A-1; 5′-GATCGGCCAAGGAGAGCATTCGATTCAAGAGATCGAATGCTCTCCTTGGCCTTTTTTGGAAA-3′ and 5′- AGCTTTTCCAAAAAAGGCCAAGGAGAGCATTCGATCTCTTGAATCGAATGCTCTCCTTGGCC-3′ for VPS4A-2; 5′- GATCGGCTGGGAACTACGAAGAATTCAAGAGATTCTTCGTAGTTCCCAGCCTTTTTTGGAAA-3′ and 5′- AGCTTTTCCAAAAAAGGCTGGGAACTACGAAGAATCTCTTGAATTCTTCGTAGTTCCCAGCC-3′ for VPS4B-1; 5′- GATCGCGGTCACTATCTAACACATTCAAGAGATGTGTTAGATAGTGACCGCTTTTTTGGAAA-3′ and 5′- AGCTTTTCCAAAAAAGCGGTCACTATCTAACACATCTCTTGAATGTGTTAGATAGTGACCGC-3′ for VPS4B-2; 5′- GATCGACATGCCTTCAGAGGATGTTCAAGAGACATCCTCTGAAGGCATGTCTTTTTTGGAAA-3′ and 5′- AGCTTTTCCAAAAAAGACATGCCTTCAGAGGATGTCTCTTGAACATCCTCTGAAGGCATGTC-3′ for VPS35-1; 5′-GATCAGTGGCAGATCTCTACGAATTCAAGAGATTCGTAGAGATCTGCCACTTTTTTTGGAAA-3′ and 5′- AGCTTTTCCAAAAAAAGTGGCAGATCTCTACGAATCTCTTGAATTCGTAGAGATCTGCCACT-3′ for VPS35-2; 5′- GATCGTTTGATACCCAGCTCTTCTTCAAGAGAGAAGAGCTGGGTATCAAACTTTTTTGGAAA-3′ and 5′-AGCTTTTCCAAAAAAGTTTGATACCCAGCTCTTCTCTCTTGAAGAAGAGCTGGGTATCAAAC-3′ for Rab9A-1; and 5′- GATCTCAACATGGGGATGGAGAATTCAAGAGATTCTCCATCCCCATGTTGATTTTTTGGAAA-3′ and 5′- AGCTTTTCCAAAAAATCAACATGGGGATGGAGAATCTCTTGAATTCTCCATCCCCATGTTGA-3′ for Rab9A-2.

For human AP-4 μ knockdown, the siRNA target sequence reported by Burgos et al. (8) was used to design complementary oligonucleotides as follows: 5′- GATCGTCTCGTTTCACAGCTCTGTTCAAGAGACAGAGCTGTGAAACGAGACTTTTTTGGAAA-3′ and 5′-AGCTTTTCCAAAAAAGTCTCGTTTCACAGCTCTGTCTCTTGAACAGAGCTGTGAAACGAGAC-3′ for AP-4 μ.

The complementary pair of DNA oligonucleotides was annealed and ligated into the linearized pSUPER.retro.puro (pSUPER) shRNA or pSUPER.retro.gfp+neo (pSUPER+GFP) expression vectors (OligoEngine) in between the BglII and HindIII sites.

ELISA, Protein Determination, and Immunoblotting. Cells were transfected in six-well plates with 3.5 μg pSUPER shRNA constructs using Lipofectamine 2000 (Life Technologies) in serum-free Opti-MEM (Life Technologies) for 24 h. For double knockdown experiments, we used 1.75 μg of each shRNA construct. Transfection media were replaced by complete media containing 4 μg/mL puromycin (Sigma-Aldrich) at 24 h posttransfection. At 72 h posttransfection, cells were trypsinized and cell numbers were measured with a Coulter Counter (Beckman Coulter).

Th same numbers of cells (6.5×10^6) were replated onto 60-mm dishes in selection media containing puromycin. At 96 h posttransfection, selection media were replaced with fresh media without puromycin, and were conditioned for 24 h. At 120 h posttransfection, conditioned media were collected with the addition of protease inhibitor mixture mini tablets (Roche). Media were diluted 10- to 20- fold (same dilution factor was used for control and knockdown samples in the same set of experiment) and subjected to $A\beta_{40}$ ELISA analysis (Life Technologies) according to the manufacturer's instructions. For immunoblotting analysis, cells were scraped and lysed in ice-cold RIPA buffer (50 mM Tris-HCl, pH 7.6, 150 mM NaCl, 0.5% sodium deoxycholate, 0.1% SDS, 1% Nonidet P-40, 5 mM EDTA, and protease inhibitor mixtures mini tablets). Lysates were centrifuged at $20,800 \times g$ at 4 °C for 30 min, and protein concentration was determined by BCA protein assay (Thermo Fisher Scientific). Equal amounts of protein samples were separated by SDS/PAGE and transferred to Immobilon-FL PVDF membranes (Millipore), and were analyzed and quantified with an Odyssey Infrared Imaging System (LI-COR). Actin or SEC23A were used as loading controls. All experiments were performed at least three times independently. Data represented as mean ± SEM were plotted and analyzed by Prism software (GraphPad) by using a paired *t* test to compare the relative amounts of $A\beta_{40}$ in control and knockdown samples.

Immunofluorescence Microscopy and Quantification. Cells were transfected in six-well plates with 3.5 μg pSUPER+GFP shRNA constructs using Lipofectamine 2000 (Life Technologies) in serum-free Opti-MEM (Life Technologies) for 24 h. For double knockdown experiments, we used 1.75 μg of each shRNA construct. Transfection medium was replaced by complete medium at 24 h posttransfection. At 96 h posttransfactions, cells were trypsinzed and replated onto polylysine-coated coverslips. At 120 h posttransfection, cells were fixed with 4% paraformaldehyde (Electron Microscopy Sciences) for 1 h at room temperature, permeabilized with 0.1% Triton X-100, stained for primary antibodies and Alexa Fluor-conjugated secondary antibodies, and mounted on microscopic slides with ProLong Gold antifade reagent containing DAPI (Life Technologies). Cells were imaged using a wide-field fluorescence microscope (AxioObserver Z1; Carl Zeiss). Images were processed and analyzed by MetaMorph image analysis software (Molecular Devices). Cells sustained knockdown as indicated by expression of GFP were selected for quantification. The extent of APP colocalization with subcellular markers Golgin 97 or EEA1 was determined by quantification of overlapping pixels in the Alexa 568 and the Alexa 647 channels. The percentage of APP pixels that overlapped with Golgin 97 or EEA1 pixels was measured and represented as mean ± SD from at least 20 cells per sample from at least two representative experiments that were performed multiple times with similar results.

ACKNOWLEDGMENTS. The authors thank Sangram S. Sisodia (University of Chicago), Wesley I. Sundquist (University of Utah), Margaret S. Robinson (University of Cambridge), and Jean-Pierre Paccaud (Drugs of Neglected Diseases Initiative, Geneva, Switzerland) for gifts of antibodies; Ann Fischer and Michelle Richner for tissue culture support; Mandy Peng for plasmid constructions; and John Tran (University of California, San Francisco), Giulia Zanetti, and Jenna McKenzie for comments on the manuscript. This work was supported by a Croucher Foundation Scholarship, Hong Kong (to R.W.C.). R.S. is an Investigator of the Howard Hughes Medical Institute and a Senior Fellow of the Miller Institute, University of California, Berkeley.

1. Small SA, Gandy S (2006) Sorting through the cell biology of Alzheimer's disease: intracellular pathways to pathogenesis. *Neuron* 52:15–31.
2. Thinakaran G, Koo EH (2008) Amyloid precursor protein trafficking, processing, and function. *J Biol Chem* 283:29615–29619.
3. Cupers P, et al. (2001) The discrepancy between presenilin subcellular localization and gamma-secretase processing of amyloid precursor protein. *J Cell Biol* 154:731–740.
4. Kim SH, Lah JJ, Thinakaran G, Levey A, Sisodia SS (2000) Subcellular localization of presenilins: Association with a unique membrane pool in cultured cells. *Neurobiol Dis* 7:99–117.
5. Kim J, et al. (2007) Biogenesis of gamma-secretase early in the secretory pathway. *J Cell Biol* 179:951–963.
6. Xu H, et al. (1997) Generation of Alzheimer beta-amyloid protein in the trans-Golgi network in the apparent absence of vesicle formation. *Proc Natl Acad Sci USA* 94: 3748–3752.
7. Siman R, Velji J (2003) Localization of presenilin-nicastrin complexes and gamma-secretase activity to the trans-Golgi network. *J Neurochem* 84:1143–1153.
8. Burgos PV, et al. (2010) Sorting of the Alzheimer's disease amyloid precursor protein mediated by the AP-4 complex. *Dev Cell* 18:425–436.
9. Lammich S, et al. (1999) Constitutive and regulated alpha-secretase cleavage of Alzheimer's amyloid precursor protein by a disintegrin metalloprotease. *Proc Natl Acad Sci USA* 96:3922–3927.
10. Carey RM, Balcz BA, Lopez-Coviella I, Slack BE (2005) Inhibition of dynamin-dependent endocytosis increases shedding of the amyloid precursor protein ectodomain and reduces generation of amyloid beta protein. *BMC Cell Biol* 6:30.
11. Perez RG, et al. (1999) Mutagenesis identifies new signals for beta-amyloid precursor protein endocytosis, turnover, and the generation of secreted fragments, including Abeta42. *J Biol Chem* 274:18851–18856.
12. Huse JT, Pijak DS, Leslie GJ, Lee VM, Doms RW (2000) Maturation and endosomal targeting of beta-site amyloid precursor protein-cleaving enzyme. The Alzheimer's disease beta-secretase. *J Biol Chem* 275:33729–33737.
13. Kinoshita A, et al. (2003) Demonstration by FRET of BACE interaction with the amyloid precursor protein at the cell surface and in early endosomes. *J Cell Sci* 116: 3339–3346.
14. Hurley JH, Hanson PI (2010) Membrane budding and scission by the ESCRT machinery: It's all in the neck. *Nat Rev Mol Cell Biol* 11:556–566.
15. Henne WM, Buchkovich NJ, Emr SD (2011) The ESCRT pathway. *Dev Cell* 21:77–91.
16. Bache KG, Raiborg C, Mehlum A, Stenmark H (2003) STAM and Hrs are subunits of a multivalent ubiquitin-binding complex on early endosomes. *J Biol Chem* 278: 12513–12521.
17. Razi M, Futter CE (2006) Distinct roles for Tsg101 and Hrs in multivesicular body formation and inward vesiculation. *Mol Biol Cell* 17:3469–3483.
18. Doyotte A, Russell MR, Hopkins CR, Woodman PG (2005) Depletion of TSG101 forms a mammalian "Class E" compartment: A multicisternal early endosome with multiple sorting defects. *J Cell Sci* 118:3003–3017.
19. Langelier C, et al. (2006) Human ESCRT-II complex and its role in human immunodeficiency virus type 1 release. *J Virol* 80:9465–9480.
20. Babst M, Katzmann DJ, Estepa-Sabal EJ, Meerloo T, Emr SD (2002) Escrt-III: An endosome-associated heterooligomeric protein complex required for mvb sorting. *Dev Cell* 3:271–282.
21. Kim SH, et al. (2001) Multiple effects of aspartate mutant presenilin 1 on the processing and trafficking of amyloid precursor protein. *J Biol Chem* 276: 43343–43350.
22. Ganley IG, Espinosa E, Pfeffer SR (2008) A syntaxin 10-SNARE complex distinguishes two distinct transport routes from endosomes to the trans-Golgi in human cells. *J Cell Biol* 180:159–172.
23. Pfeffer SR (2009) Multiple routes of protein transport from endosomes to the trans Golgi network. *FEBS Lett* 583:3811–3816.
24. Bonifacino JS, Hurley JH (2008) Retromer. *Curr Opin Cell Biol* 20:427–436.
25. Vieira SI, et al. (2010) Retrieval of the Alzheimer's amyloid precursor protein from the endosome to the TGN is S655 phosphorylation state-dependent and retromer-mediated. *Mol Neurodegener* 5:40.
26. Sullivan CP, et al. (2011) Retromer disruption promotes amyloidogenic APP processing. *Neurobiol Dis* 43:338–345.
27. Puertollano R, Aguilar RC, Gorshkova I, Crouch RJ, Bonifacino JS (2001) Sorting of mannose 6-phosphate receptors mediated by the GGAs. *Science* 292:1712–1716.
28. Waguri S, et al. (2003) Visualization of TGN to endosome trafficking through fluorescently labeled MPR and AP-1 in living cells. *Mol Biol Cell* 14:142–155.
29. Small SA, et al. (2005) Model-guided microarray implicates the retromer complex in Alzheimer's disease. *Ann Neurol* 58:909–919.
30. Rogaeva E, et al. (2007) The neuronal sortilin-related receptor SORL1 is genetically associated with Alzheimer disease. *Nat Genet* 39:168–177.
31. Andersen OM, et al. (2005) Neuronal sorting protein-related receptor sorLA/LR11 regulates processing of the amyloid precursor protein. *Proc Natl Acad Sci USA* 102: 13461–13466.
32. Offe K, et al. (2006) The lipoprotein receptor LR11 regulates amyloid beta production and amyloid precursor protein traffic in endosomal compartments. *J Neurosci* 26: 1596–1603.
33. Fjorback AW, et al. (2012) Retromer binds the FANSHY sorting motif in SorLA to regulate amyloid precursor protein sorting and processing. *J Neurosci* 32:1467–1480.